ADVANCES IN ATMOSPHERIC SCIENCES, VOL. 40, JANUARY 2023, 1–5

• News & Views •

Detection of Anthropogenic CO_2 Emission Signatures with TanSat CO_2 and with Copernicus Sentinel-5 Precursor (S5P) NO_2 Measurements: First Results

Dongxu YANG*[1], Janne HAKKARAINEN[2], Yi LIU[1], Iolanda IALONGO[2], Zhaonan CAI[1], and Johanna TAMMINEN[2]

[1]*Institute of Atmospheric Physics*, *Chinese Academy of Sciences*, *Beijing* 100029, *China*

[2]*Finnish Meteorological Institute*, *Helsinki FI*-00560, *Finland*

(Received 29 August 2022; revised 8 October 2022; accepted 10 October 2022)

ABSTRACT

China's first carbon dioxide (CO_2) measurement satellite mission, TanSat, was launched in December 2016. This paper introduces the first attempt to detect anthropogenic CO_2 emission signatures using CO_2 observations from TanSat and NO_2 measurements from the TROPOspheric Monitoring Instrument (TROPOMI) onboard the Copernicus Sentinel-5 Precursor (S5P) satellite. We focus our analysis on two selected cases in Tangshan, China and Tokyo, Japan.We found that the TanSat XCO_2 measurements have the capability to capture the anthropogenic variations in the plume and have spatial patterns similar to that of the TROPOMI NO_2 observations. The linear fit between TanSat XCO_2 and TROPOMI NO_2 indicates the CO_2-to-NO_2 ratio of 0.8×10^{-16} ppm (molec cm^{-2})$^{-1}$ in Tangshan and 2.3×10^{-16} ppm (molec cm^{-2})$^{-1}$ in Tokyo. Our results align with the CO_2-to-NO_x emission ratios obtained from the EDGAR v6 emission inventory.

Key words: TanSat, CO_2, Remote sensing, city carbon emission, climate change

Citation: Yang, D. X., J. Hakkarainen, Y. Liu, I. Ialongo, Z. N. Cai, and J. Tamminen, 2023: Detection of anthropogenic CO_2 emission signatures with TanSat CO_2 and with Copernicus Sentinel-5 Precursor (S5P) NO_2 measurements: First results. *Adv. Atmos. Sci.*, **40**(1), 1–5, https://doi.org/10.1007/s00376-022-2237-5.

1. Introduction

By absorbing infrared radiation, greenhouse gases trap heat in the Earth's atmosphere, which would otherwise escape into space, and greenhouse gas concentrations in the atmosphere have increased since the onset of the industrial revolution. In the 2015 United Nations Climate Change Conference held in Paris, participants agreed to reduce greenhouse gas emissions to prevent an average global surface temperature increase of more than 1.5°C. Hence, mitigating or slowing down global warming represents a challenge faced by the global population in the 21st century. Concentrations of carbon dioxide (CO_2) have risen by more than 40% due to anthropogenic activities such as fossil fuel combustion and land-use change. The emissions related to the combustion of fossil fuels are particularly localized, with urban areas being the dominant contributor responsible for more than 70% of global emissions.

Even though global economies are struggling due, in part, to the recovery from the impact of COVID-19, in 2021, fossil-fuel-related CO_2 emissions have shown an increase of 5% with an uncertainty of ±5% (Friedlingstein et al., 2022). Large uncertainty remains in fossil-fuel emission estimates when focused on specific countries (Andres et al., 2014), and uncertainties are even larger than expected for cities (Ciais et al., 2014; Gately et al., 2015; Miller and Michalak, 2017; Gately and Hutyra, 2017; Oda et al., 2018; Gurney et al., 2019). For example, one investigation indicates a 20.4% variation in the fossil-fuel emission estimates of Los Angeles, while variations exceeding 200% were found in Beijing (Han et al., 2020). The uncertainty mainly comes from two parts, the remaining bias in the emission inventory statistics, for example, less than optimal estimations of energy consumption and emission factors (Liu et al., 2015), and the inability to adequately capture the rapidly increasing magnitude of fossil-fuel consumption related to economic growth, which is not updated in a timely manner.

* Corresponding author: Dongxu YANG
Email: yangdx@mail.iap.ac.cn

To better understand the uncertainty of carbon emissions (sources) and sinks, satellite missions dedicated to atmospheric greenhouse measurements have been developed in the last decade. China's Global Carbon Dioxide Monitoring Scientific Experimental Satellite (TanSat) was launched in December 2016 after Japan's Greenhouse gases Observing SATellite (GOSAT, 2009) (Kuze et al., 2009) and NASA's Orbiting Carbon Observatory-2 (OCO-2, 2014) (Crisp et al., 2017) mission. Similar to the OCO-2 mission, TanSat has a hyperspectral grating spectrometer covering the near-infrared (NIR) and short-wave infrared (SWIR) regions that are sensitive to CO_2 absorption (Liu and Yang, 2016). The nadir footprint size of TanSat measurement is ~2×2 km^2, and it has nine footprints across the track in a frame, which means TanSat has the potential to capture anthropogenic emission enhancements in a city and downwind of a power station.

The CEOS Chair commissioned the Atmospheric Composition Virtual Constellation (AC-VC) to define a global architecture for monitoring atmospheric greenhouse gas concentrations and their fluxes from space (Crisp et al., 2018). Quantifying anthropogenic CO_2 emissions is one of the most important requirements of the global greenhouse gas monitoring system that increases the verification support (MVS) capacity to support the Paris Agreement. Carbon dioxide measurements alone cannot provide enough information to screen out the atmospheric background, which includes CO_2 turbulence from the natural carbon cycle; therefore, it is useful to coordinately use measurements of short-lived anthropogenic tracers, e.g., NO_2 and CO. In this study, we introduce the first attempts to use TanSat CO_2 measurements to detect anthropogenic CO_2 emission signatures together with the Copernicus Sentinel-5 Precursor (S5P) NO_2 measurements.

2. Satellite data

2.1. *TanSat XCO_2 retrieval*

TanSat XCO_2 data are retrieved by the Institute of Atmospheric Physics Carbon dioxide retrieval Algorithm for Satellite remote sensing (IAPCAS) (Yang et al., 2018, 2020, 2021). The standard TanSat XCO_2 retrieval has been introduced and released to the public (http://www.chinageoss.cn/tansat/index.html). The cross footprint bias significantly impacts research that compares city-based emissions to global carbon flux inversions. The bias correction method used in the TanSat v2 data product cannot meet the requirements of this study due to the bias correction reference to the global absolute bias. The relative biases between a footprint with a scale of tens of kilometers to a footprint with a scale of hundreds of kilometers have not been efficiently resolved. In this study, we introduce a new bias correction strategy. To reduce a cross-footprint bias, we first apply a dynamic bias-related parameter selection to a cloud-screened data product. The bias has been separated into absolute bias and relative bias components. The former part has been corrected to a TCCON measurement which uses a coupling method similar to TanSat v2 processing. For each footprint, the relative bias correction parameters are selected from a rank of bias relativity, including solar zenith angle, surface pressure, albedo, aerosol optical depth, cloud optical depth, spectrum correction coefficient, etc. Additionally, in the relative bias correction, we apply a 0.1° moving window cross-footprint bias correction for each footprint. This special bias-corrected XCO_2 data product is only used in this study, and the bias correction method will be considered in the next version of TanSat XCO_2 data production [Fig. S1 in the electronic supplementary material (ESM)].

2.2. *TROPOMI/Sentinel-5P NO_2 data*

The TROPOspheric Monitoring Instrument (TROPOMI) is the sole satellite instrument onboard the Copernicus Sentinel-5 Precursor (S5P) satellite. It flies on a sun-synchronous polar orbit with an equatorial overpass time at 1330 LST (LST = UTC + 8), close to the TanSat mission equatorial overpass time. One of the advantages of the TROPOMI tropospheric NO_2 observations compared to its predecessors is the high spatial resolution (currently 5.5 km by 3.5 km at nadir) which enables the detection of NO_2 plumes. As nitrogen oxides (NO_x = NO + NO_2) are often co-emitted with CO_2, this data can be used to facilitate the identification and analysis of the CO_2 plumes. For example, TROPOMI NO_2 data were used to derive the plume width of the CO_2 plume using the cross-sectional flux method (Reuter et al., 2019) and to analyze the NO_x-to-CO_2 emission ratio together with OCO-2 XCO_2 observations of the Matimba power station in South Africa (Hakkarainen et al., 2021). Previously, tropospheric NO_2 observations had been used, for example, to characterize global XCO_2 anomalies (Hakkarainen et al., 2016).

3. Results

Here, we analyze two TanSat overpasses over anthropogenic emission plumes. In the first case (6 May 2018), TanSat captures an XCO_2 enhancement near Tangshan, China, while in the second case (29 March 2018), it detects an emission plume originating from Tokyo, Japan.

Tangshan: Figure 1 illustrates the case of Tangshan on 6 May 2018. The map in Fig. 1 (left panel) shows the TROPOMI tropospheric NO_2 columns overlapped by the TanSat XCO_2 observations. The arrows indicate the ERA5 wind fields. For illustrative purposes, we removed the local background from the TanSat XCO_2 observations. The background is

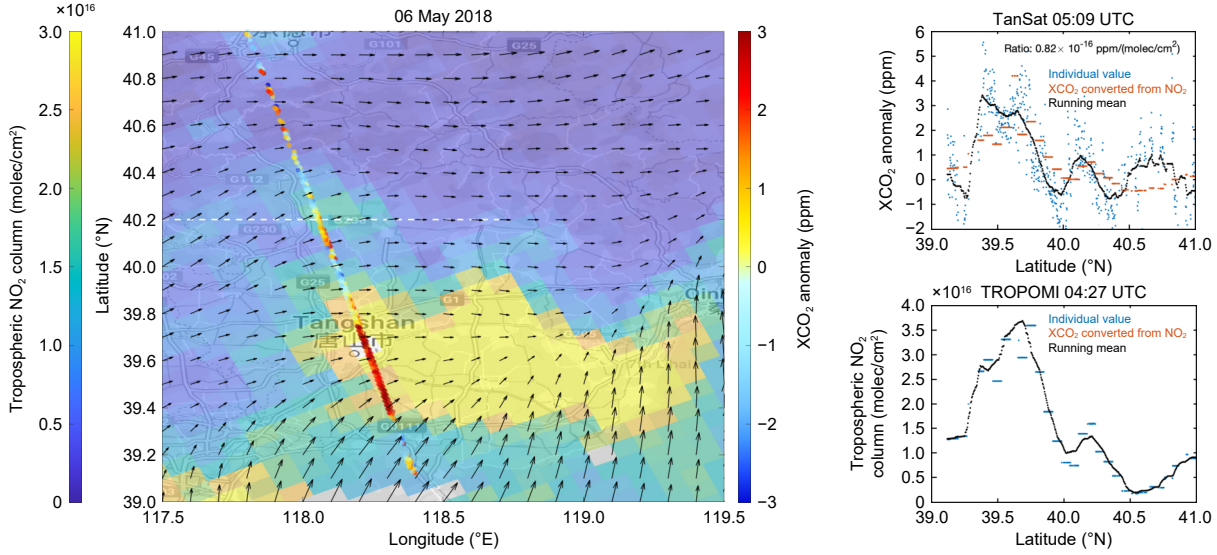

Fig. 1. The left panel illustrates TROPOMI NO_2 observations overlapped by TanSat XCO_2 observation near Tangshan (China) on 6 May 2018. ERA5 wind fields are shown as arrows. The XCO_2 background is calculated as a median, north of the white dashed line. The right panels (top and bottom) show the XCO_2 and NO_2 observations (respectively) along the TanSat track. The black dots indicate the running mean. Orange colors indicate the XCO_2 converted from NO_2 tropospheric columns via a linear fit.

calculated from the median of the XCO_2 values north of the white dashed line in Fig. 1, and we thus consider this to be the local XCO_2 anomaly. With respect to this background, the largest enhancements near Tangshan are about 4–5 ppm. The co-located TROPOMI tropospheric NO_2 columns indicate values of 3.5×10^{16} molec cm^{-2}. Figure 1 (right, top, and bottom panels, respectively) shows the NO_2 and XCO_2 observations (blue dots) along the TanSat track, while the black dots indicate the running means. We observe two enhancements at about 39.5°N and 40.1°N from both datasets, corresponding to one emission area near Tangshan and another about 60 km north). We calculated the linear fit between TROPOMI NO_2 and TanSat XCO_2 observations to transform NO_2 tropospheric columns into XCO_2 (orange dots in Fig. 1; top right panel). The slope of the linear fit indicates the CO_2-to-NO_2 ratio (Hakkarainen et al., 2019, 2021) for this case is about 0.8×10^{-16} ppm $(\text{molec cm}^{-2})^{-1}$, roughly corresponding to the ratio of the CO_2 and NO_2 peak values near Tangshan. The correlation coefficient of the linear fit is 0.54.

Tokyo: Figure 2 shows the case of the Tokyo plume on 29 March 2018. We again calculate the background north of the white dashed line and consider local XCO_2 anomalies. We note that the enhancements are spread over a wide city area. The highest running mean values are between 2–3 ppm. The highest TROPOMI NO_2 enhancements co-located with TanSat are about 1×10^{16} molec cm^{-2}. In addition to the main enhancement east of Tokyo, another smaller enhancement is visible, e.g., near latitude 36.5°N. The linear fit between TanSat XCO_2 and TROPOMI NO_2 indicates that the CO_2-to-NO_2 ratio is about 2.3×10^{-16} ppm $(\text{molec cm}^{-2})^{-1}$, which roughly corresponds to the ratio of the peak values. This ratio is about 2–3 times higher than the ratio observed near Tangshan. The correlation coefficient of the linear fit is 0.47. The main reason for the higher CO_2-to-NO_2 ratio is the higher CO_2-to-NO_x emission ratio in Tokyo with respect to Tangshan. For example, considering the pixels ±0.5° around Tangshan and Tokyo in the EDGAR v6 emission inventory (Crippa et al., 2021) gives an emission ratio of about 400 for Tangshan and 1000 for Tokyo. In addition, the higher ratio in Tokyo could be partly due to the distance from the source, as the NO_2 lifetime is relatively short (about 4 hours). However, in both cases, the linear fit is calculated over a large area.

4. Outlook

In this study, we introduced the first attempt to use TanSat measurements to detect anthropogenic CO_2 emission signatures. Carbon dioxide enhancements of 2–3 ppm in Tokyo and 3–4 ppm in Tangshan have been observed by TanSat nadir measurements, corresponding to enhancements in the S5P NO_2 measurement. To accurately measure anthropogenic CO_2 signals, the coverage, footprint size, and repeat cycle of satellite observations need to be improved. The next generation of China's Global Carbon Dioxide Monitoring Satellite mission, TanSat-2, is now in the design phase. The target measurement will focus on cities with an 800–1000 km swath to record the gradient of XCO_2 from its central to rural areas using an imaging process and a 500 m footprint size to improve the emission estimation accuracy. TanSat-2 will not be a single satellite but a constellation distributed into at least two orbits in the morning and afternoon to cover a city or point source twice daily. The

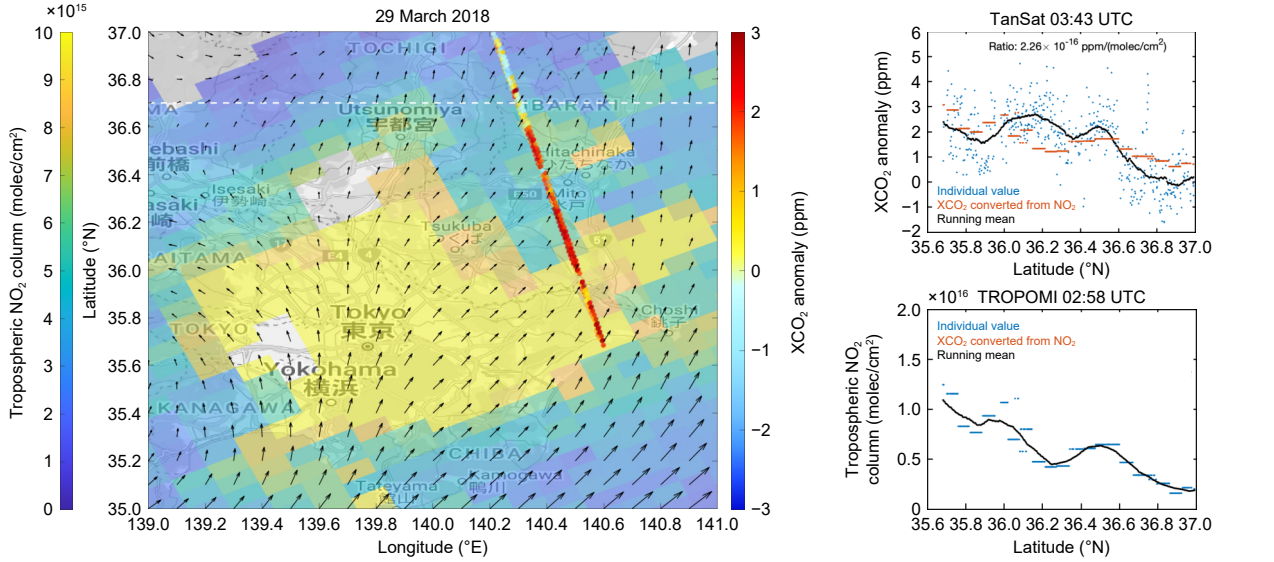

Fig. 2. Same as Fig. 1, but for Tokyo on 29 March 2018.

co-located measurements of NO_2 help constrain anthropogenic CO_2 emissions from the total CO_2 budget. Hence, a NO_2-detecting instrument will be on board the TanSat-2 satellite to identify the emission plume and help constrain anthropogenic emissions in the atmospheric inversion.

Acknowledgements. This work is supported by the National Key Research And Development Plan (2019YFE0127500), International Partnership Program of the Chinese Academy of Sciences (060GJHZ2022070MI). The authors thank the Finland-China mobility cooperation project funded by the Academy of Finland (No. 348596) and the Key Research Program of the Chinese Academy of Sciences (ZDRW-ZS-2019-1). Financial support for the Academy of Finland (No. 336798) is kindly acknowledged. The authors thank the TanSat mission, and the support from everyone that worked with TanSat mission is highly appreciated.

Electronic supplementary material: Supplementary material is available in the online version of this article at https://doi.org/10.1007/s00376-022-2237-5.

REFERENCES

Andres, R. J., T. A. Boden, and D. Higdon, 2014: A new evaluation of the uncertainty associated with CDIAC estimates of fossil fuel carbon dioxide emission. *Tellus B*, **66**(1), 23616, https://doi.org/10.3402/tellusb.v66.23616.

Ciais, P., and Coauthors, 2014: Current systematic carbon-cycle observations and the need for implementing a policy-relevant carbon observing system. *Biogeosciences*, **11**(13), 3547–3602, https://doi.org/10.5194/bg-11-3547-2014.

Crippa, M., and Coauthors, 2021: GHG emissions of all world countries. EUR 30831 EN, Publications Office of the European Union, Luxembourg, 2021, ISBN 978-92-76-41547-3, doi:10.2760/074804, JRC126363. [Available online from https://publications.jrc.ec.europa.eu/repository/handle/JRC126363]

Crisp, D., and Coauthors, 2017: The on-orbit performance of the Orbiting Carbon Observatory-2 (OCO-2) instrument and its radiometrically calibrated products. *Atmospheric Measurement Techniques*, **10**, 59–81, https://doi.org/10.5194/amt-10-59-2017.

Crisp, D., and Coauthors, 2018: A constellation architecture for monitoring carbon dioxide and methane from space. [Available online from https://ceos.org/document_management/Virtual_Constellations/ACC/Documents/CEOS_AC-VC_GHG_White_Paper_Publication_Draft2_20181111.pdf]

Friedlingstein, P., and Coauthors, 2022: Global carbon budget 2021. *Earth System Science Data*, **14**, 1917–2005, https://doi.org/10.5194/essd-14-1917-2022.

Gately, C. K., and L. R. Hutyra, 2017: Large uncertainties in urban-scale carbon emissions. *J. Geophys. Res.: Atmos.*, **122**(20), 11 242–11 260, https://doi.org/10.1002/2017JD027359.

Gately, C. K., L. R. Hutyra, and I. Sue Wing, 2015: Cities, traffic, and CO_2: A multidecadal assessment of trends, drivers, and scaling relationships. *Proceedings of the National Academy of Sciences of the United States of America*, **112**(16), 4999–5004, https://doi.org/10.1073/pnas.1421723112.

Gurney, K. R., J. Liang, D. O'Keeffe, R. Patarasuk, M. Hutchins, J. Huang, P. Rao, and Y. Song, 2019: Comparison of global downscaled versus bottom-up fossil fuel CO_2 emissions at the urban scale in four U.S. urban areas. *J. Geophys. Res.: Atmos.*, **124**, 2823–2840, https://doi.org/10.1029/2018JD028859.

Hakkarainen, J., I. Ialongo, and J. Tamminen, 2016: Direct space-based observations of anthropogenic CO_2 emission areas from OCO-2. *Geophys. Res. Lett.*, **43**(21), 11 400-11 406, https://doi.org/10.1002/2016GL070885.

Hakkarainen, J., I. Ialongo, S. Maksyutov, and D. Crisp, 2019: Analysis of four years of global XCO_2 anomalies as seen by orbiting carbon observatory-2. *Remote Sensing*, **11**, 850, https://doi.org/10.3390/rs11070850.

Hakkarainen, J., M. E. Szeląg, I. Ialongo, C. Retscher, T. Oda, and D. Crisp, 2021: Analyzing nitrogen oxides to carbon dioxide emission ratios from space: A case study of Matimba Power Station in South Africa. *Atmos. Environ.: X*, **10**, 100110, https://doi.org/10.1016/j.aeaoa.2021.100110.

Han, P. F., and Coauthors, 2020: A city-level comparison of fossil-fuel and industry processes-induced CO_2 emissions over the Beijing-Tianjin-Hebei region from eight emission inventories. *Carbon Balance and Management*, **15**, 25, https://doi.org/10.1186/s13021-020-00163-2.

Kuze, A., H. Suto, M. Nakajima, and T. Hamazaki, 2009: Thermal and near infrared sensor for carbon observation Fourier-transform spectrometer on the Greenhouse Gases Observing Satellite for greenhouse gases monitoring. *Appl. Opt.*, **48**(35), 6716–6733, https://doi.org/10.1364/AO.48.006716.

Liu, Y., and D. X. Yang, 2016: Advancements in theory of GHG observation from space. *Science Bulletin*, **61**(5), 349–352, https://doi.org/10.1007/s11434-016-1022-1.

Liu, Z., and Coauthors, 2015: Reduced carbon emission estimates from fossil fuel combustion and cement production in China. *Nature*, **524**, 335–338, https://doi.org/10.1038/nature14677.

Miller, S. M., and A. M. Michalak, 2017: Constraining sector-specific CO_2 and CH_4 emissions in the US. *Atmos. Chem. Phys.*, **17**, 3963–3985, https://doi.org/10.5194/acp-17-3963-2017.

Oda, T., S. Maksyutov, and R. J. Andres, 2018: The Open-source Data Inventory for Anthropogenic CO_2, version 2016 (ODIAC2016): A global monthly fossil fuel CO_2 gridded emissions data product for tracer transport simulations and surface flux inversions. *Earth System Science Data*, **10**(1), 87–107, https://doi.org/10.5194/essd-10-87-2018.

Reuter, M., M. Buchwitz, O. Schneising, S. Krautwurst, C. W. O'Dell, A. Richter, H. Bovensmann, and J. P. Burrows, 2019: Towards monitoring localized CO_2 emissions from space: Co-located regional CO_2 and NO_2 enhancements observed by the OCO-2 and S5P satellites. *Atmospheric Chemistry and Physics*, **19**, 9371–9383, https://doi.org/10.5194/acp-19-9371-2019.

Yang, D., and Coauthors, 2020: Toward high precision XCO_2 retrievals from TanSat observations: Retrieval improvement and validation against TCCON measurements. *J. Geophys. Res.: Atmos.*, **125**, e2020JD032794, https://doi.org/10.1029/2020JD032794.

Yang, D. X., Y. Liu, Z. N. Cai, X. Chen, L. Yao, and D. R. Lu, 2018: First global carbon dioxide maps produced from TanSat measurements. *Adv. Atmos. Sci.*, **35**, 621–623, https://doi.org/10.1007/s00376-018-7312-6.

Yang, D. X., and Coauthors, 2021: A new TanSat XCO_2 global product towards climate studies. *Adv. Atmos. Sci.*, **38**, 8–11, https://doi.org/10.1007/s00376-020-0297-y.